Journal of Thermal Analysis and Calorimetry (2021) 145:51–58
https://doi.org/10.1007/s10973-020-09681-0

High-temperature transformations of Zr-pillared bentonite

Juan Manuel Martinez[1] · Maria Susana Conconi[1] · Fernando Booth[2] · Nicolás M. Rendtorff[3]

Received: 19 November 2019 / Accepted: 7 April 2020 / Published online: 23 April 2020

Abstract
A Zr-modified bentonite (B-OHZr) obtained by intercalation of OH-Zr species was obtained, and its thermal transformations at > 800 °C were studied. Raw clay and B-OHZr were characterized by X-ray diffraction, thermogravimetric and differential thermal analysis, and its sintering behavior was studied by hot-stage microscopy. Two Zr-based phases—tetragonal zirconia and zircon—were observed in thermally treated B-OHZr with a sharp decrease in amorphous glassy phase in comparison with the parental clay. An increase in refractoriness was observed in B-OHZr, enabling the sintering of samples up to 1300 °C, while the parental clay bloated and deformed with thermal treatment. The Zr interlayering enhanced the refractoriness at high temperatures of the parental clay, eliminating thermal expansion (bloating) and enabling sintering at $T > 1000$ °C. The observed features and thermochemical processes enlighten the temperature usage range of these kinds of materials. Finally these results yield promising features for potential use of these clays for the preparation of ceramic materials with zircon content.

Keywords Bentonite · PILCs · Zirconia · Thermal behavior · Thermal resistance

Introduction

Montmorillonite (Mt) is a 2:1 type clay mineral which belongs to the smectite group. Mt has a characteristic two-dimensional structure, where an aluminum octahedral sheet is sandwiched between two silica tetrahedral sheets [1, 2]. Si^{+4} and Al^{+3} cations in the tetrahedral and octahedral sheets, respectively, can be isomorphically replaced, thus generating negative charges in the layer. Cations in the interlayer spacing, such as Na^{+}, K^{+}, Ca^{+2}, Mg^{+2}, compensate these negative charges. The cation exchange capability of these clays, i.e., the replacement of these cations with other species, enables the possibility of Mt-derived composites with a wide array of applications, such as additives in drilling fluids, as hosts for drug delivery, as supports for catalyst, to name a few of them [3–6].

An important application of this type of clay, after intercalation with inorganic polyhydroxylated species and thermal treatment, is the preparation of pillared interlayered clays (PILCs). Inorganic species include, among others, Al, Zr, Ti and Fe [7–10]. Thermal treatment of these intercalated species is performed at 350–750 °C, with this temperature depending on the type of clay, the intercalated species and the intercalation procedure. PILCs have a wide array of uses in catalysis and adsorbents due to their high specific surface and thermal stability [8, 11, 12].

As expected, the chemical composition of the interlayered clay (precursor) increases its content of the interlayered specie, which modifies not only its textural properties, but also affects its thermal behavior and other properties. Characterization of these materials is mainly done using 4 techniques—X-ray diffraction (XRD), nitrogen adsorption, infrared spectroscopy and nuclear magnetic resonance—assisted by many other techniques (to a lesser extent) [13]. Thermal behavior is analyzed by differential thermal analysis, differential scanning calorimetry and thermogravimetry up to 750–850 °C, temperature at which a series of reactions transforms the metastable polycations into stable oxyhydroxide phases, "bridging" the interlayered species and

✉ Juan Manuel Martinez
juanmartinez@cetmic.unlp.edu.ar

[1] CETMIC Centro de Tecnología de Recursos Minerales y Cerámica (CIC-CONICET La Plata), Cno. Centenario y 506 M.B. Gonnet (1897), Buenos Aires, Argentina

[2] Universidad Nacional del Chaco Austral, Comandante Fernandez 755, Presidente Roque Saenz Peña, Argentina

[3] Departamento de Química, Facultad de Ciencias Exactas, Universidad Nacional de La Plata, 47 y 115, La Plata, 1900 Buenos Aires, Argentina

the clay layer, giving the materials a good thermal resistance while maintaining a high specific surface [13, 14]. However, further heating at higher temperatures causes the collapse of such bridges and the loss of the characteristic clay mineral structure. This collapse is not well described, as in the present work we pretend to contribute to understand its principal features.

Although the collapse of the clay mineral structure causes a loss of the specific surface in PILCs, interesting features arises because of the thermal treatment at high temperatures. For example, Al-pillared montmorillonites develop crystalline phases with important technological properties, such as mullite which has a good mechanical properties even at high temperatures; and cordierite, which, although has a lower mechanical resistance, has higher capacity as a thermal insulator [15, 16]. This type of clay has shown good properties for its use as ceramic coatings [17]. To the best of our knowledge, other Zr-based PILCs have not been studied after thermal treatment at > 1000 °C. One of such PILCs is the Zr-pillared clays, which could develop interesting Zr-based crystalline phases through thermal treatment; a higher refractoriness can be presumed. The thermal behavior of the oxide–clay mixture has not been reported as well. Mecif et al. [18] have studied the interaction between three kaolinitic clays with fine powdered zirconia (ZrO_2) when thermally treated, observing zircon ($ZrSiO_4$) formation at temperatures > 1200 °C. Zircon exhibits attractive properties, such as resistance to alkali corrosion, low thermal expansion coefficient (4.1×10^{-6} K^{-1}), low heat conductivity [18, 19].

This provides novel information about the thermal behavior and physicochemical characteristics of the developed Zr clay, mainly about the crystalline phases developed through thermal treatment, which could enable to establish typical usage limits and potential new uses for this type of clay.

The objective of this work was to study the thermal, chemical, structural and sintering behavior of Zr-PILCs precursors prepared from an unpurified bentonite, thermally treated at temperatures up to 1300 °C. The focus of this work was the studying of the distinct features of Zr-PILCs at high temperatures compared with those of its parent clay. Raw precursor and bentonite were characterized by simultaneous differential thermal analysis and thermogravimetry (DTA-TG), X-ray fluorescence (XRF) and XRD. Thermal behavior was assessed by a multi-technique approach, sintering behavior was studied by hot-stage microscopy (HSM), and crystalline phases developed at high temperatures were followed by XRD and Rietveld refinement of thermally treated samples. This will enlighten design strategies of these kinds of materials.

Materials and experimental procedures

Materials

The clay used in this work was a bentonite from the province of San Juan, Argentina. This clay has been characterized in previous works [20] and is composed mainly of montmorillonite, with traces of quartz and feldspar. The structural formula of the montmorillonite clay mineral in this sample is $\left[\left(Si_{3.94}Al^{IV}_{0.06}\right)\left(Al^{VI}_{10.36}Fe_{0.06}Mg_{0.60}\right)O_{10}(OH)_2\right]$.

The Zr-based reagent used for the intercalated clay was a partially hydrolyzed solution prepared from 0.1 M of $ZrOCl_2$ aged for 1 day at 60 °C. It has been reported that said solution consists of tetramers with the formula $[Zr_4(OH)_{24}(H_2O)_{10}]^{+2}$, in which two of the Zr ions have a positive charge and the other two are neutral [21].

Synthesis of the Zr-intercalated bentonite

The preparation of the Zr-intercalated clay was carried out as reported by Volzone and Hipedinger [21]. The bentonite was contacted with the OH-Zr species solution mentioned above for 24 h; the solid was washed with distilled water to remove excess electrolytes. The material thus obtained, designated as B-OHZr, was allowed to dry at room temperature. B-OHZr powder samples (M: 100) were thermally treated in an electric oven at a heating rate of 5 °C min^{-1} up to 1000, 1100, 1200 and 1300 °C for 1 h for further structural analysis.

Raw characterization (XRF–XRD)

Powder XRD patterns of the raw clay and B-OHZr were recorded using a diffractometer Philips with goniometer 3020 and PW3710 controller in the range of 3º–70º (2θ). The measurements were taken at 40 mA and 40 kV with CuKα radiation using a Ni filter.

TG/DTA analysis of B and B-OHZr was determined using a Rigaku (Thermo Plus Evo, 220 V 50 Hz) simultaneous thermal analysis equipment using α-Al_2O_3 as reference at a heating rate of 10 °C min^{-1} up to 1300 °C.

Sintering/thermal treatment (DTA-TG, hot-stage microscopy)

Sintering studies of the samples were performed using a hot-stage microscope (HSM). Cylindrical specimens (5 mm high and 3 mm in diameter) were prepared by uniaxial pressing of powdered B and B-OHZr. They were placed vertically on the sample holder of the heating microscope oven (L74 Linseis) and were synthesized with a heating ramp of 10 °C min^{-1} up

to 1300 °C. The temperature was recorded with a Pt–Rh type S thermocouple. The images captured with the digital camera in the microscope were configured in such a way as to obtain a record of one shot per degree centigrade. Changes of the cross-sectional surface area of the samples (S) in the course of their heating compared with the cross-sectional surface area (S_0) of the samples at the starting temperature were determined analyzing the digital images using the software provided by the equipment.

Disc-shaped samples (18.0 mm diameter, 1.5 mm thickness) of B and B-OHZr were uniaxially die pressed at 30 MPa with the addition of 1% mass of water, with a pressing displacement rate of 0.05 mm s^{-1}.

The disc-shaped samples were employed for the sintering study, with 5 °C min^{-1} as heating rate and 120 min of plateau at 950 and 1200 °C, respectively, in air atmosphere, in an electric kiln. Porosity and density of the sintered samples were employed as sintering parameters; textural properties were measured by the Archimedes method.

Materials and methods

Chemical analysis of samples was done by X-ray fluorescence (XRF, Shimadzu 165 EDX800-HD). Initial and resultant crystalline phases were analyzed by XRD (Philips 3020 equipment) with CuKα radiation in Ni filter at 40 kV to 20 mA, with 2θ between 3° and 70°, 2 s steps of 0.04°. The XRD patterns were analyzed with the program FullProf (version 4.90, July 2010) which is a multipurpose profile-fitting program, including Rietveld refinement to perform phase quantification. Formerly the phases were identified using phase analysis software (X'Pert HighScore, version 2.1.2) with the PDF-2 database (ICDD PDF-2). In particular, the amorphous phase was quantified by the Le Bail method, in which this phase is refined as a crystalline silica one with extremely low crystallite size [22, 23].

Results and discussion

Composition and crystalline structure of B and B-OHZr

The parental clay, B, was investigated in previous studies [17]. The Zr-interlayered clay showed, besides an increase in the amount of ZrO_2 present in the sample, a decrease in CaO and NaO_2 content. Reduction of the interlayer cations content (Ca^{2+} and Na^{+}) and increase in Zr content after treatment with the OH-Zr solution suggest that the interlayer cations were displaced by the OH-Zr species in the clay mineral [8, 24]. According to a previously reported study [24], the species found in the solution are identified as tetramers of the formula $[Zr_4(OH)_{14}(H_2O)_{10}]^{2+}$. The high amount of OH^- and H_2O on its structural formula results in a lost on ignition increase after treatment of the clay with these species.

XRD patterns of both B and B-OHZr samples (Fig. 1a) revealed the presence of a montmorillonite clay mineral, with low amounts of quartz and feldspar. However, the d(001) shifted from 1.48 nm in B to 2.01 nm in B-OHZr (Fig. 1b). The sample B-OHZr has a calculated interlayer spacing of 1.05 nm. As estimated from their structural information, the Zr tetramers have a molecular dimension of 1 $nm^2 \times 1$ nm^2 for an average square configuration and 0.45 nm thick [25]. With these dimensions, it can be introduced into the interlayer spacing, displacing the exchange cations of the montmorillonite forming a monolayer of complexes normal to the sheet of the clay mineral or as a double layer of flat complexes, in both cases, giving an interlayer spacing, approximately 1 nm.

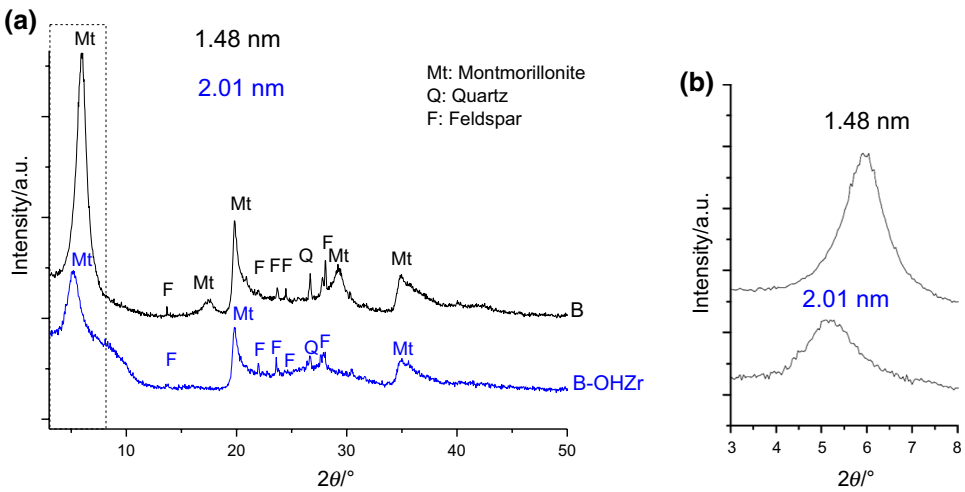

Fig. 1 **a** XRD patterns of raw clay and B-OHZr and **b** d(001)

Thermal and sintering behavior

The intercalation of OH-Zr species caused changes in the DTA curve of B-OHZr in comparison with the precursor clay (Fig. 2a). The B sample was only tested up to 1000 °C because of the glass formation. The first endothermic peak centered at 100 °C, associated with the loss of adsorbed water and hydration of the interlayer species widened slightly for the B-OHZr sample. The second endothermic peak, which is associated with the dehydroxylation of the clay mineral, moved to lower temperatures (480 °C) [26, 27]. These lower temperatures for the dehydroxylation reaction of the clay mineral in the intercalated samples would indicate that the intercalated species affected the hydroxyl groups of the octahedral layer of the clay [28]. Possibly, the low pH of the $ZrOCl_2$ solution used for sample preparation favored the protonation and dissociation of structural groups or dissolution of the montmorillonite structure with release of metal ions (Al, Mg) from the octahedral layer [28]. DTA curves also show an endo-exothermic peak centered at around 800–850 °C. This *S*-shaped peak corresponds to the collapse of the clay mineral structure and the appearance of new crystalline phases [26], and it is centered at slightly higher values for B-OHZr (840 °C) than B (860 °C). This slight shift is attributed to the interlayered Zr species transformation into a ZrO_2-like pillar, which supports the structure of said clay, thus preventing an early collapse [24].

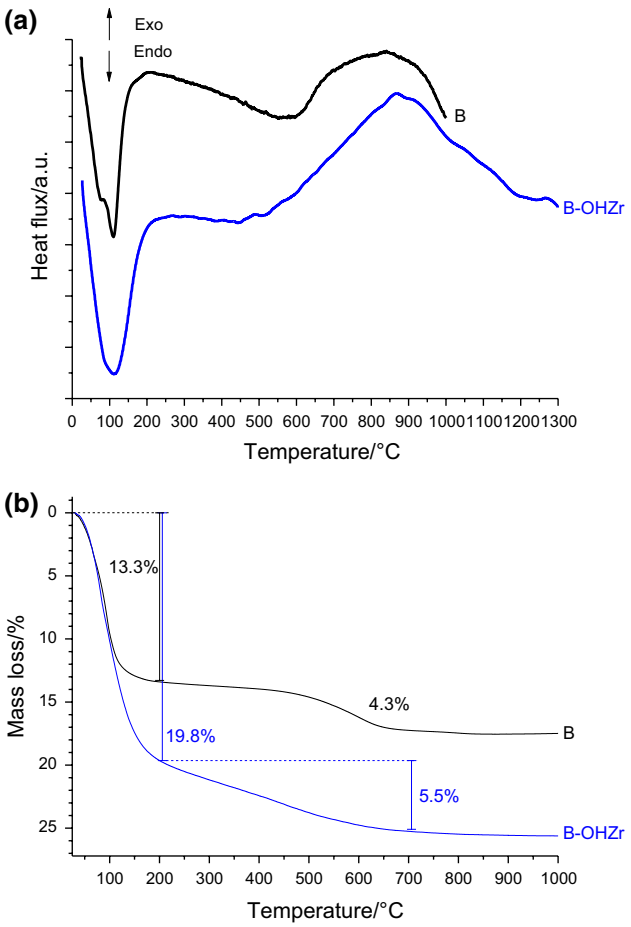

Fig. 2 **a** DTA and **b** TG curves of B and B-OHZr

The TG curve of B showed a mass loss of 13.3% up to 200 °C which, as mentioned above, is attributed to the loss of water absorbed and to the water of hydration of the interchangeable cations. B-OHZr showed a mass loss of 19.8% in the same temperature range. This greater value is related to the intercalated polymeric OH-Zr species [24, 28], which have a higher content of OH-groups and water molecules in comparison with the interlayer cations (Na^+, K^+, Ca^{2+}) of the original bentonite. The dehydration and dehydroxylation of these polymeric species during the thermal treatment are reflected in higher mass losses for the B-OHZr.

The sample B presented a mass loss of 4.3% in a relatively narrow temperature range (500–700 °C), associated with the removal of structural hydroxyls for B, while B-OHZr showed a higher mass loss (5.5%) in a wider range of temperatures (200–700 °C). This value is higher in B-OHZr (5.5%) because the dehydroxylation of the Zr-interlayered species goes up to higher temperatures and overlaps with the removal of the hydroxyls of the montmorillonite layer. No significant mass changes above 800 °C were recorded in any of the samples.

Evolution of the cross section of cylindrical specimens of B and B-OHZr with the temperature during the test (Fig. 3) was registered using a hot-stage microscope. Sample B at 1200 °C underwent an expansion process with a morphological change from cylindrical to roughly spherical, before collapsing at higher temperatures. Panna et al. [29] observed similar behaviors for clays with high smectite content, associating this behavior with the formation of liquid by the thermal treatment at high temperature of this mineral. Temperatures > 900 °C contribute to the development of a liquid phase rich in high viscosity silica, which has the ability to retain gases trapped inside the pores of the probes which expands during the sintering of the material, producing the expansion of it ("bloating") and becomes spherical under the action of the surface tension of the melt [30]. An increase in temperature causes the decrease in the viscosity of the liquid phase, which leads to the escape of the gases generated, and the collapse of the structure and, at higher temperatures, the complete fusion of the material.

B-OHZr samples do not deform up to the maximum test temperature of 1300 °C. Comparing the chemical composition (Table 1), the reduction of the content of flux oxides (Na_2O, K_2O, CaO) and the enrichment in Zr, whose oxides have high melting points (ZrO_2), could explain the increase in thermal stability of B-OHZr samples.

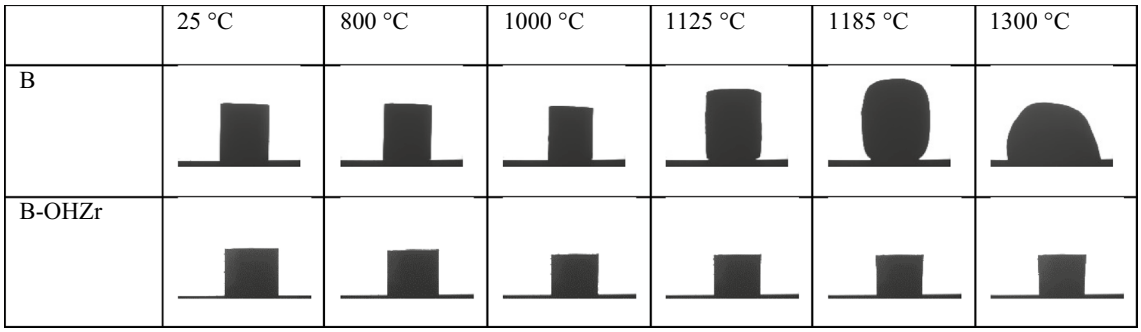

Fig. 3 Evolution of the cross section of samples of B and B-OHZr during the thermal treatment in a hot-stage microscope

Table 1 Chemical composition of B and B-OHZr (mass%) obtained by XRF

	SiO_2	Al_2O_3	TiO_2	Fe_2O_3	MgO	K_2O	CaO	Na_2O	ZrO_2	LOI (1000 °C)
B	49.89	18.05	0.18	1.09	5.75	0.54	1.22	2.08	< 0.02	21.11
B-OHZr	45.60	15.06	0.21	0.93	4.26	0.36	0,28	0.03	7.14	26.08

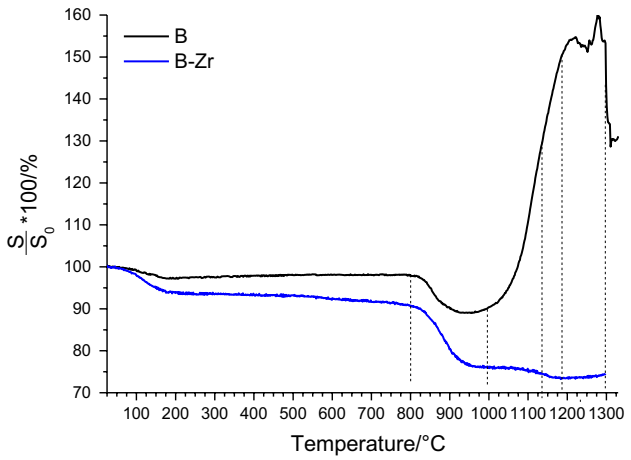

Fig. 4 Specific area as a function of the heating program showing dimensional changes of B and B-OHZr samples

Figure 4 shows the dimensional changes of the cross-sectional area compared with S_0 of the samples by heating microscopy of the specimens prepared with B and B-OHZr. In the same can be seen a clear similarity between the curves up to 800 °C for both samples. The bentonite B presents a contraction of S/S_0 of approximately 3% up to 200 °C which is associated with the loss of water absorbed from the clay mineral. No additional dimension changes were determined up to 800 °C. From this temperature onwards, the beginning of a rapid contraction is observed, which increases to a value of S/S_0 of 90.0% at 930 °C, contraction attributable to the structural collapse of montmorillonite and the beginning of sintering. At temperatures above 930 °C an expansion up to 1200 °C, temperature at which a decrease in the value of S/S_0 begins. The "noise" in the last part of the curve is explained by the sudden burst of air bubbles inside the sample.

For B-OHZr, an initial contraction of 5% at low temperatures, similar to that of B, is observed, which intensifies from 800 °C to 10% for 1000 °C. However, further thermal treatment causes additional sintering, without any expansion observed, reaching a maximum contraction at 1200 °C, with a relative height of 84.1%.

As the analysis of the TG curves for both samples in this temperature range did not reveal any mass loss (Fig. 2a), the difference in behavior can be attributed to the combination of several phenomena such as structural destruction, the start of the formation of new and different crystalline phases, as well as the formation of different amounts of liquid phase since they can act in a simultaneous way.

Resulting crystalline phases of sintered powders by X ray diffraction

Figure 5a, b shows the XRD patterns of B and B-OHZr thermally treated up to 1300 °C. Both samples showed no montmorillonite reflections, as this structure is destroyed due to the collapse of the clay mineral structure at lower temperatures [26, 27]. They also developed a broad band centered at around 22° 2θ due to the presence of an amorphous phase [31] and showed the presence of unreacted feldspar (anorthite) and quartz. Thermal treatment above 800 °C causes a silica-rich liquid phase to be formed due to the melting of the silica tetrahedral in the montmorillonite sheet and alkalis present. In particular, the B-OHZr sample also developed amorphous bands centered at tetragonal-zirconia (t-ZrO_2) peaks, probably denoting a short-range ordering of a tetragonal-zirconia-like structure. This could be due to

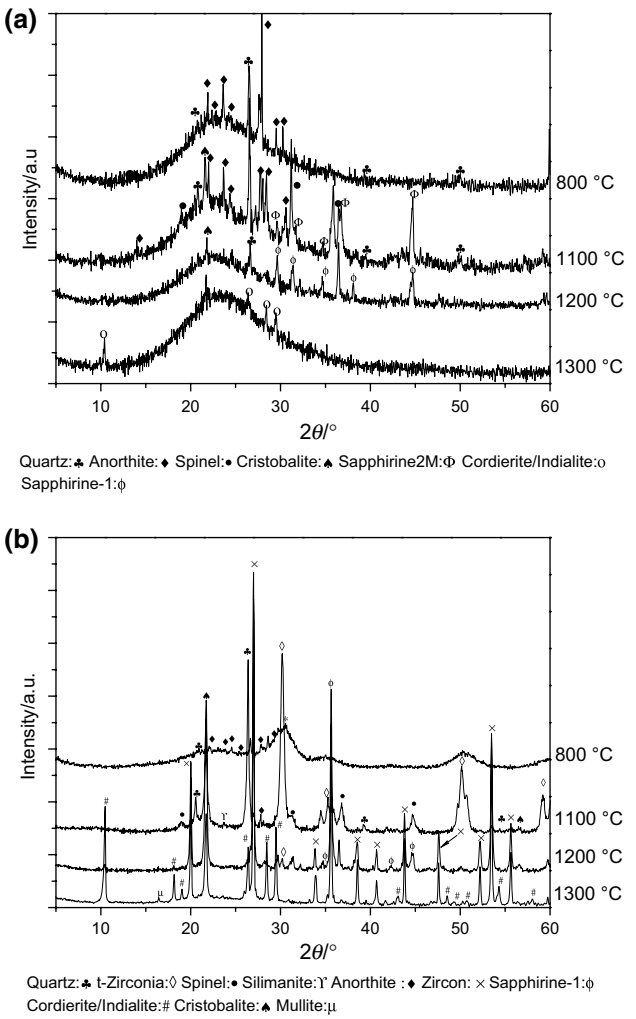

Fig. 5 XRD plot of **a** B and **b** B-OHZr thermally treated at different temperatures

the stabilization effect of the Mg present in the clay mineral structure [32].

The crystalline phases developed by B were those typical of a montmorillonite with a clay mineral structure rich in Mg [27]. At 1100 °C spinel ($MgAl_2O_4$), sapphirine ($A_{15}Mg_3$)(Al_4Si_2)O_{20} and cristobalite (SiO_2) were developed, and minor amounts of unreacted feldspar (anorthite—(Ca,Na)$(Al,Si)_2Si_2O_8$) and quartz (SiO_2) were present. At 1200 °C, feldspar reflections disappeared, cristobalite remained while cordierite ($Mg_2Al_4Si_5O_{18}$) reflections were observed. At 1300 °C, the sample is mainly amorphous, with small peaks of cordierite. The development of mullite, which is usually observed in thermally treated clays, was not observed on this sample. This can be explained by the low amount of Al in the clay mineral due to a high amount of isomorphic replacement of structural Al^{+3} with Mg^{+2} in the octahedral sheet [33, 34], which favored instead the development of cordierite.

Table 2 Crystalline phases and Rietveld refinement cell parameters of B and B-OHZr

Sample	B-OHZr	
Firing temperature/°C	1200	1300
RWP (residual weight profile)	27.0	15.4
Cristobalite 1PDF: 01-082-0512		
a (Å)	5.0802(53)	5.0317(14)
c (Å)	6.9966(11)	7.0665(64)
Cristobalite 2PDF: 01-082-0512		
a (Å)	5.0125(29)	–
c (Å)	6.98732(6)	–
Zircon PDF: 00-006-0266		
a (Å)	6.5989(19)	6.6015(4)
c (Å)	5.9762(2)	5.9829(5)
Sapphirine-1 PDF: 00-044-1430		
a (Å)	9.9680(84)	–
b (Å)	10.3491(25)	–
c (Å)	8.5999(8)	–
Indialite PDF: 01-082-1884		
a (Å)	–	9.7746(17)
c (Å)	–	9.3262(2)
Mullite PDF: 00-015-0776		
a (Å)	–	7.5456(108)
b (Å)	–	7.6984(11)
bc (Å)	–	2.8930(2)

In comparison, the crystalline phases developed by B-OHZr regarding the presence of crystalline phases without Zr content showed differences than those developed by B. Sapphirine was first observed at 1200 °C, and small amounts of mullite were observed at 1300 °C. In general, the crystallinity of the samples was much higher. B-OHZr developed two Zr-based crystalline phases: tetragonal-zirconia (ZrO_2) and zircon ($ZrSiO_4$), though zirconia appeared at 1100 °C only, while zircon peaks intensity increased with higher temperatures.

Rietveld refinement results: cell parameters and phase quantifications

The results of the Rietveld refinement for main crystalline phases of the samples thermally treated at 1200 and 1300 °C are shown in Table 2. Although cell parameters of all the crystalline phases were refined, only the more representative and abundant in each sample are described due to the low reliability of the parameters from minor crystalline phases. Table 3 shows the quantified crystalline and amorphous phases in each material. Global estimated standard deviations derived from the estimated standard deviation on individual scale factors, for the respective phases, are presented in the table as well.

Table 3 Rietveld quantification (mass%) of B and B-OHZr

Sample		B		B-OHZr	
Firing temperature/°C		1200	1300	1200	1300
R_{Wp} (residual weight profile)		27.8	20.9	27.0	15.4
Phase	Formula				
Quartz	SiO_2	1.3(2)	–	–	–
Sapphirine-It	$(Al_5Mg_3)(Al_4Si_2)O_{20}$	13.3(2)	–	20.5(4)	–
Cristobalite	SiO_2	0.4(4)	–	7.8(1)	7.2(1)
Cristobalite(2)	SiO_2	–	–	18.7(2)	–
Mullite	$3Al_2O_3{\cdot}2SiO_2$	–	–	–	4.2(2)
Cordierite/indialite	$Mg_2Al_{3.96}Si_{5.04}O_{18}$	1.2(1)	3.6(3)	3.7(1)	38.4(3)
Zirconia	ZrO_2	–	–	0.7(1)	–
Zircon	$ZrSiO_4$	–	–	32.1(3)	27.4(2)
Amorphous phase (Le Bail)	Mainly SiO_2	83.9(1)	96.4(9)	16.4(8)	22.8(5)

The Rwp parameter values were in all cases below 30, assuring the reliability of the refinements for this kind of materials [1, 35].

The shape of the cristobalite peaks for sample B-OHZr thermally treated at 1200 °C could not be satisfactorily adjusted with a single contribution. As proposed for similar materials [36, 37], two different cristobalite structures were proposed for the refinement. This could possibly be explained by the presence of separate phases: one obtained from the thermal decomposition and recombination of the montmorillonite, while the other is obtained from thermal transformations of the quartz present on the parental clay.

Zircon present in B-OHZr samples was accompanied with a decrease in amorphous phase content in comparison with the parental clay samples. The highly reactive silica glassy phase formed could react with the zirconia present, thus deriving in a higher degree of crystallinity, also enhanced by the removal of flux oxides in favor of Zr during the synthesis of B-OHZr (Table 1).

Textural properties of the sintered ceramics

In order to illustrate the effect in the refractoriness of the PILC strategy, sintered B and B-OHZr samples were thermally treated at maximum sintering temperature without deforming, as observed in the HSM curves. B samples were sintered up to 950 °C, while B-OHZr samples were sintered up 1200 °C for 1 h. Both samples presented low open porosity values (< 3%), although the density of B-OHZr sample was more than twice than that of the B sintered sample (Table 4). This could be attributed to a high amount of enclosed porosity on the B sintered sample, as shown by its expansion due to bloating measured by hot-stage microscopy (Fig. 4).

Table 4 Textural properties of the sintered ceramics B and B-OHZr

Sample	Open porosity/%	Err	Dens/g cm^{-3}	Err
B	2.21	0.02	1.53	0.15
B-OHZr	2.33	0.02	4.06	0.15

Conclusions

- Zr-interlayered clays were synthetized and its high-temperature properties were characterized. Thermochemical processes and macroscopic effects were described and compared with the parental clay.
- Nanocrystalline tetragonal zirconia was observed in the Zr-intercalated clay. At higher temperatures, Zr-derived phases, i.e., zirconia and zircon, were found, and its content was dependent with the treatment temperature and the amount of amorphous phase was lower than in the raw bentonite. The performed structural refinement permitted to deeply characterize the developed crystalline phases, with define the technological features of the materials.
- The Zr interlayering enhanced the refractoriness at high temperatures of the parental clay, eliminating thermal expansion (bloating) and enabling sintering at $T > 1000$ °C.
- The observed features and thermochemical processes enlighten the temperature usage range of this kind of materials. Finally, these results yield promising features for potential use of these clays for the obtention of ceramic materials with zircon content.

Acknowledgements This work was supported by CONICET. This work has been partially supported by Nano-Petro FONARSEC Project

2012 (ANPCyT). N.R. thanks FONCyT-BID PICT 2016-1193. Juan Manuel Martinez thanks CONICET for the scholarship.

References

1. Andrini L, Toja RM, Gauna MR, Conconi MS, Requejo FG, Rendtorff N. Extended and local structural characterization of a natural and 800 °C fired Na-montmorillonite–Patagonian bentonite by XRD and Al/Si XANES. Appl Clay Sci. 2017;137:233–40.
2. Brindley G. Quantitative X-ray mineral analysis of clays. In: Brindley G, Brown G, editors. Crystal structures of clay minerals and their X-ray identification. London: Mineralogical Society; 1980.
3. Jayrajsinh S, Shankar G, Agrawal YK, Bakre L. Montmorillonite nanoclay as a multifaceted drug-delivery carrier: a review. J Drug Deliv Sci Technol. 2017;39:200–9.
4. Li L, Song Y, Jiang B, Wang K, Zhang Q. A novel oxygen carrier for chemical looping reforming: $LaNiO_3$ perovskite supported on montmorillonite. Energy. 2017;131:58–66.
5. Zhong H, Qiu Z, Huang W, Cao J. Shale inhibitive properties of polyether diamine in water-based drilling fluid. J Petrol Sci Eng. 2011;78(2):510–5.
6. Zhuang G, Zhang Z, Peng S, Gao J, Pereira FA, Jaber M. The interaction between surfactants and montmorillonite and its influence on the properties of organo-montmorillonite in oil-based drilling fluids. Clays Clay Miner. 2019;67(3):190–208.
7. Herney-Ramirez J, Vicente MA, Madeira LM. Heterogeneous photo-Fenton oxidation with pillared clay-based catalysts for wastewater treatment: a review. Appl Catal B. 2010;98(1–2):10–26.
8. Kloprogge J. Synthesis of smectites and porous pillared clay catalysts: a review. J Porous Mater. 1998;5(1):5–41.
9. Vaughan DEW, Lussier RJ. Preparation of molecular sieves based on pillared interlayered clays (PILC). In: Rees LVC, editor. Proceedings of 5th international conference on zeolites. London: Heyden Press; 1980. p. 94–101.
10. Gil A, Korili SA, Trujillano R, Vicente MA. Pillared clays and related catalysts. Berlin: Springer; 2010.
11. Li J, Hu M, Zuo S, Wang X. Catalytic combustion of volatile organic compounds on pillared interlayered clay (PILC)-based catalysts. Curr Opin Chem Eng. 2018;20:93–8.
12. Zhang Y, Zhang Y, Liu T, Ai Z, Yang S. Synthesis of lanthanum modified titanium pillared montmorillonite and its application for removal of phosphate from wastewater. Sci Adv Mater. 2017;9(3–4):673–81.
13. Gil A, Korili SA, Trujillano R, Vicente MA. A review on characterization of pillared clays by specific techniques. Appl Clay Sci. 2011;53(2):97–105.
14. Vicente M, Gil A, Bergaya F. Pillared clays and clay minerals. In: Bergaya F, Lagaly G, editors. Developments in clay science. Amsterdam: Elsevier; 2013. p. 523–57.
15. Martinez JM, Volzone C, Garrido LB. Thermal transformations up to 1200 °C of Al-pillared montmorillonite precursors prepared by different OH–Al polymers. J Therm Anal Calorim. 2016. https://doi.org/10.1007/s10973-016-5938-0.
16. Kingery WD. Introduction to ceramics. New York: Wiley; 1960.
17. Martinez JM, Volzone C, Garrido LB. Evaluation of polymeric Al-modified bentonite for its potential application as ceramic coating. Appl Clay Sci. 2017;149:20–7.
18. Mecif A, Soro J, Harabi A, Bonnet JP. Preparation of mullite- and zircon-based ceramics using kaolinite and zirconium oxide: a sintering study. J Am Ceram Soc. 2010;93(5):1306–12.
19. Rendtorff N, Garrido L, Aglietti E. Thermal behavior of mullite–zirconia–zircon composites. influence of zirconia phase transformation. J Therm Anal Calorim. 2011;104(2):569–76.
20. Vidal N, Volzone C. Influence of organobentonite structure on toluene adsorption from water solution. Mater Res. 2012;15(6):944–53.
21. Volzone C, Hipedinger NE. Influence of hydrolyzed zirconium solutions on the OH-Zr-montmorillonite. Clays Clay Miner. 1999;47(1):109.
22. Conconi MS, Gauna MR, Serra MF, Suarez G, Aglietti EF, Rendtorff N. Quantitative firing transformations of a triaxial ceramic by X-ray diffraction methods. Cerâmica. 2014;60(356):524–31.
23. Le Bail A. Modelling the silica glass structure by the Rietveld method. J Non Cryst Solids. 1995;183(1–2):39–42.
24. Jung H, Paek S-M, Yoon J-B, Choy J-H. Zr K-edge XAS study on ZrO_2-pillared aluminosilicate. J Porous Mater. 2007;14(4):369–77.
25. Clearfield A, Vaughan PA. The crystal structure of zirconyl chloride octahydrate and zirconyl bromide octahydrate. Acta Crystallogr A. 1956;9(7):555–8.
26. Mackenzie R, Caillere S. Thermal analysis, DTA, TG, DTG. In: van Olphen H, Fripiat JJ, editors. Data handbook for clay materials and other non-metallic minerals, vol. 442. Oxford: Pergamon Press; 1979. p. 243–84.
27. Grim REK, Kulbicki G. Montmorillonite: high temperature reactions and classification. Am Mineral. 1961;46:1329–69.
28. Kou MS, Mendioroz S, Guijarro M. A thermal study of Zr-pillared montmorillonite. Thermochim Acta. 1998;323(1–2):145–57.
29. Panna W, Szumera M, Wyszomirski P. The impact of modifications of the smectite-bearing raw materials on their thermal expansion ability. J Therm Anal Calorim. 2016;123(2):1153–61.
30. Dumitrache RL, Teoreanu I. Melting behaviour of feldspar porcelain glazes. UPB Sci Bull. 2006;68(1):3–16.
31. Gavin P, Chevrier V, Ninagawa K, Gucsik A, Hasegawa S. Experimental investigation into the effects of meteoritic impacts on the spectral properties of phyllosilicates on Mars. J Geophys Res Planets. 2013;118(1):65–80.
32. Duwez P, Odell F, Brown FH. Stabilization of zirconia with calcia and magnesia. J Am Ceram Soc. 1952;35(5):107–13.
33. Volzone C, Garrido LB. High temperature structural modifications of intercalated montmorillonite clay mineral with OH-Al polymers. Procedia Mater Sci. 2012;1:164–71.
34. Li YW, Schulthess CP, Sahoo S, Alpay SP. Influence of octahedral cation distribution in montmorillonite on interlayer hydrogen counter-ion retention strength via first-principles calculations. Clays Clay Miner. 2019;67:439–48.
35. Bonetto RD, Zalba PE, Conconi MS, Manassero M. The Rietveld method applied to quantitative phase analysis of minerals containing disordered structures. Revista Geológica de Chile. 2003;30(1):103–15.
36. Butler M, Dyson D. The quantification of different forms of cristobalite in devitrified alumino-silicate ceramic fibres. J Appl Crystallogr. 1997;30(4):467–75.
37. Hernández MF, Conconi MS, Cipollone M, Herrera MS, Rendtorff N. Ceramic behavior of ball clay with gadolinium oxide (Gd_2O_3) addition. Appl Clay Sci. 2017;146:380–7.